JBC Papers in Press. Published on January 18, 2017 as Manuscript M116.766311
The latest version is at http://www.jbc.org/cgi/doi/10.1074/jbc.M116.766311

Structure-activity relationship of α mating pheromone from the fungal pathogen *Fusarium oxysporum*

Stefania Vitale[1,*], Angélica Partida-Hanon[2,*], Soraya Serrano[2], Álvaro Martínez-del-Pozo[3], Antonio Di Pietro[1], David Turrà[1#] and Marta Bruix[2#]

From the [1]Department of Genetics, Campus de Excelencia Internacional Agroalimentario ceiA3, Universidad de Córdoba, 14071 Córdoba, Spain, the [2]Department of Biological Physical Chemistry, Institute of Physical Chemistry Rocasolano, CSIC, Serrano 119, 28006 Madrid, Spain, the [3]Department of Biochemistry and Molecular Biology I, Faculty of Chemistry, Complutense University, 28040 Madrid, Spain.

*These authors contributed equally to the work. [#]Co-corresponding authors.

Running title: *Fusarium oxysporum α-pheromone structure-activity*

To whom correspondence should be addressed: David Turrà, Phone: +34-957-218981, E-mail: ge3tutud@uco.es; Marta Bruix, Phone: +34-915-619400, E-mail: mbruix@iqfr.csic.es.

Keywords: *Fusarium oxysporum*; α-pheromone; chemotropism; hyphal growth inhibition

Abstract

During sexual development, ascomycete fungi produce two types of peptide pheromones termed a and α. The α pheromone from the budding yeast *Saccharomyces cerevisiae*, a thirteen residue peptide which elicits cell cycle arrest and chemotropic growth, has served as paradigm for the interaction of small peptides with their cognate G protein-coupled receptors (GPCRs). However, no structural information is currently available for α pheromones from filamentous ascomycetes, which are significantly shorter and share almost no sequence similarity with the *S. cerevisiae* homolog. High-resolution structure of synthetic α-pheromone from the plant pathogenic ascomycete *Fusarium oxysporum* revealed the presence of a central β-turn resembling that of its yeast counterpart. Disruption of the fold by D-alanine substitution of the conserved central Gly_6-Gln_7 residues or by random sequence scrambling demonstrated a crucial role for this structural determinant in chemoattractant activity. Unexpectedly, the growth inhibitory effect of *F. oxysporum* α-pheromone was independent of the cognate GPCR Ste2 and of the central β-turn but instead required two conserved Trp_1-Cys_2 residues at the N-terminus. These results indicate that, in spite of their reduced size, fungal α-pheromones contain discrete functional regions with a defined secondary structure that regulate diverse biological processes such as polarity reorientation and cell division.

Mating pheromone α from the baker's yeast *Saccharomyces cerevisiae* has served as a model for studying the interaction of small peptides with G protein-coupled receptors (GPCRs) (1). Like most ascomycete fungi, *S. cerevisiae* cells of different mating types secrete small peptide pheromones (α and a) which function as sexual chemoattractants and are sensed by the cognate plasma membrane GPCRs Ste2 and Ste3, respectively (2). Ligand binding to the receptor elicits a range of cellular responses including G1 cell cycle arrest, formation of a polarized cell projection (known as a shmoo) and chemotropic growth towards the pheromone of the opposite mating type (3-5).

The mature α-pheromone of *S. cerevisiae* is a thirteen residue peptide with the sequence WHWLGLKPGQPMY (6). The central residues Pro_8-Gly_9 were proposed to form a Type II β-turn necessary to orient the N- and C-terminal ends during the interaction with the Ste2 receptor and to adapt to the conformational changes when the receptor switches to an active state (1,7,8). Alanine replacement of these central residues, which is expected to destabilize the TypeII β-turn, leads to a reduction in pheromone-receptor affinity (1,9). Besides this central region, the residues close to the C-terminus are important for physical interaction with Ste2, since replacement by alanines caused an up to 3000-fold decrease in receptor affinity and loss of growth arrest (1). Similarly, in the dimorphic human pathogen *Candida albicans*, α-pheromone tridecapeptides with di-alanine substitutions at the C-terminal positions 10-12 largely lost the ability to induce pheromone-mediated processes such as mating and biofilm formation (10). On the other hand, the N-terminus of *S. cerevisiae* α-factor plays a major role in receptor activation and downstream signaling events. Alanine scanning of this region resulted in modified peptides which still bound strongly to Ste2, but failed to exert biological activity. Interestingly, these analogs function as antagonists of α-pheromone in shmoo formation, growth arrest and gene induction assays (1).

The function of α pheromones in sexual development appears to be broadly conserved in ascomycetes and has been experimentally demonstrated for a number of species (11). Interestingly, α-pheromone peptides from filamentous ascomycetes share low to no sequence similarity with yeast α-pheromone, tend to be significantly shorter (typically 10 amino acids) and often carry conserved Trp_1-Cys_2 and Gly_6-Gln_7 residues at their N-terminus and central region, respectively (12,13). The structure-function relationship for this type of α-pheromones has not been investigated so far.

Here we present an extensive biophysical characterization and high-resolution structure of synthetic α-pheromone of *Fusarium oxysporum*, a highly destructive ascomycete plant pathogen that attacks over a hundred different crop species and has also been reported as an emerging pathogen of humans (14). *F. oxysporum* was recently shown to encode a predicted α-pheromone peptide with chemoattractant activity (12). We show that, similar to its yeast

counterpart, *F. oxysporum* α-pheromone adopts a β-turn structure in water which becomes more globular in the presence of intracellular-like cosolvents. Using di-alanine substitution as well as a scrambled derivative of the peptide, we demonstrate a crucial role for the central Gly_6-Gln_7 residues in α-pheromone bending and chemoattractant activity. We further show that α-pheromone inhibits hyphal growth of *F. oxysporum*, and that the inhibitory function is independent of the plasma membrane GPCR Ste2 and of the central Gly_6-Gln_7 residues but instead requires the conserved Trp_1-Cys_2 residues at the N-terminus.

Results

Chemoattractant activity of F. oxysporum α-pheromone requires the central Gly_6-Gln_7 residues

The synthetic *F. oxysporum* α-pheromone decapeptide WCTWRGQPCW was previously shown to elicit chemotropic growth in *F. oxysporum* germ tubes, exhibiting a bell-shaped dose-response curve (12). We performed alanine substitution of Gly_6-Gln_7, which are broadly conserved in α-pheromones of filamentous ascomycetes. The D-$Ala_{6,7}$ analog showed a dramatically reduced chemotropic activity which was similar to that of the randomly scrambled peptide (Fig 1A-B). Both of these variants elicited a weak but significant response in the wild type, but not in the *ste2Δ* strain (Fig 1C), indicating that they are still able to bind Ste2, possibly with decreased receptor affinity By contrast, alanine substitution of the N-terminal Trp_1-Cys_2 residues which are also conserved across ascomycetes, did not significantly affect chemoattractant activity (Fig. 1A). Thus, while the central Gly_6-Gln_7, but not the the N-terminal Trp_1-Cys_2 residues of α-pheromone are strictly required for chemoattractant activity.

Growth inhibitory activity of F. oxysporum α-pheromone requires the N-terminal Trp_1 and Cys_2 but not the central Gly_6-Gln_7 residues

In *S. cerevisiae* α-pheromone induces transient cell cycle arrest and growth inhibition (3-5). To test whether *F. oxysporum* α-pheromone exerts an analogous effect, we determined germ tube length as well as the number of hyphal compartments and nuclei in the absence or presence of synthetic α-pheromone. Germ tubes exposed to a gradient of 378 μM α-pheromone showed a significant decrease in the number of hyphal cell compartments and nuclei, resulting in significantly shorter hyphae compared to germ tubes exposed to trypsin-treated α-pheromone (negative control; $P < 0.0001$) (Fig. 2A, C, E). Interestingly, growth inhibition by α-pheromone was still active in the *ste2*Δ mutant (negative control; $P \leq 0.0029$) (Fig. 2B, D). Similarly to the native α-pheromone, the D-$Ala_{6,7}$ analog induced a significant reduction in average cell/nuclear division and hyphal length whereas the scrambled peptide and the D-$Ala_{1,2}$ analog lacked an inhibitory effect (versus α–pheromone, $P < 0.0001$) (Fig. 3A-C). Thus, the N-terminal Trp_1-Cys_2 but not the central Gly_6-Gln_7 residues are required for the growth inhibitory activity of α-pheromone in a Ste2-independent manner.

Peptide oligomerization

Small peptides in solution tend to be unstable and often oligomerize, giving rise to larger aggregates. Since the presence of two SH-free Cys residues in *F. oxysporum* α-pheromone suggested that it could form oligomeric structures through the formation of intermolecular disulfide bonds, we tested the presence of possible oligomers in solution by HPLC fractionation. In all cases, only a single peptide species was detected, and DTT treatment did not modify the HPLC behaviour (Fig. 4A). We conclude that the α-pheromone peptide remained monomeric when newly prepared. These results also demonstrate that the Cys residues do not establish intermolecular or intramolecular disulfide bonds, which is in agreement with the NMR data shown below. The finding that *F. oxysporum* α-pheromone and the scrambled peptide did not elute at identical retention times might imply that they adopt different conformations. The higher retention time of the scrambled peptide suggests that it is slightly more hydrophobic than the natural fungal pheromone.

Secondary structure: effect of salts and pH

Figure 4B shows the far-UV CD spectra of *F. oxysporum* α-pheromone and the three modified sequences in water and TFE mixtures. Due to the high abundance of aromatic residues which absorb in the same wavelength range,

quantification of the secondary structure populations was meaningless to perform. However, in all cases, CD data in water were compatible with an equilibrium of conformations with the presence of different contributions of β-turns. On the other hand, the use of TFE as a cosolvent stabilizes intramolecular hydrogen bonds in peptides and proteins and has been used to mimic low dielectric environments such as those with high concentrations of macromolecules and other cosolvents encountered in a cell (15). Moreover, in many cases H_2O/TFE mixtures were shown to stabilize pre-existing secondary structures in short linear peptides (16,17). In contrast to helical peptides, where 30% TFE typically increases the strength of CD minima at 208 and 222 nm, we found that the intensity of the spectral minima in α-pheromone was reduced. This change was less evident in the D-$Ala_{1,2}$ and D-$Ala_{6,7}$ peptides, where the band centred around 200 nm is smaller. While these differences are difficult to interpret due to possible opposing spectral contributions from aromatic and amide groups, we attribute the result to the presence of the D-Ala residues which produce a positive CD signal, while L-amino acids produce negative bands (18).

The CD spectra of *F. oxysporum* α-pheromone and the scrambled peptide did not change significantly upon addition of up to 200 mM NaCl, $CaCl_2$ or $MgCl_2$ (data not shown). This indicates that structure of the isolated peptide in aqueous solution is not affected by the presence of Cl^-, Na^+, Ca^{+2} or Mg^{+2} ions. Moreover, both the α-pheromone and the scrambled peptide showed a conformational transition corresponding to a pKa value of about 9.0, which can be attributed to the deprotonation of the NH_2-terminal group, though contribution of Cys side-chains ionization cannot be discarded. As expected from the nature of the individual side-chains of the amino acids that constitute the two peptides, no major changes were observed between pH 3.0 and 8.0. Thus, although the two peptides have different far-UV CD spectra and different conformational populations in equilibrium, the behaviour of these conformations against pH follows an identical variation pattern.

NMR assignment

It was previously reported that the tendency of linear peptides to form secondary structures can be confirmed by plotting ΔδHα, ΔδCα and ΔδCβ as a function of peptide sequence (19). We thus obtained ^1H and ^{13}C NMR chemical shifts for α-pheromone and the modified peptides (see Materials and Methods for details). Because aromatic amino acid rings cause major distortions in the chemical shift values due to the ring current effects (20), the large proportion of tryptophan residues (3/10 in the wild type, scrambled and D-$Ala_{6,7}$, 2/10 in D-$Ala_{1,2}$ peptides) made it difficult to extract conformational tendencies and to quantify populations from Δδ data. Thus, calculation of the 3D structures on the basis of the NOE data was mandatory to obtain information about the structure of α-pheromone peptides in solution.

NMR chemical shifts can be used to monitor the oxidation state of cysteine side chains, because Δδ between oxidized and reduced forms of $^{13}C_\beta$ is large (10-13 ppm) in comparison with the aromatic side chain effects. The measured $^{13}C_\beta$ chemical shifts of C2, C9 and C5, C6 were between 27.7 and 28.9 ppm (Fig. 5A), in agreement with values reported for reduced Cys. The expected value for the $^{13}C_\beta$ nuclei in the oxidized state should be close to 41.1 ppm (21). These data are in line with those obtained by HPLC, confirming the reduced state of all cysteines (C2 and C9 in α-pheromone and D-$Ala_{6,7}$; C5 and C6 in the scrambled peptide; C9 in D-$Ala_{1,2}$) and the absence of inter- or intra-disulphide bonds under the conditions used in this study.

X-P trans/cis conformational equilibrium in solution

In all cases, two different sets of signals were present in the NMR spectra, corresponding to the X-P *trans/cis* bond conformational equilibrium (Fig. 5B). The chemical shift difference between Pro $^{13}C\beta$ and $^{13}C\gamma$ carbons (22) ($\delta C\beta - \delta C\gamma \approx 4{,}5$ ppm) and the characteristic sequential NOEs observed between the Hα proton of X(i-1) and the Hδ and Hδ' protons of P(i), confirmed the *trans* rotamer as the major species. However, the populations varied between the different peptides. In the α-pheromone and the D-$Ala_{1,2}$ analog in H_2O, the Q7-P8 *trans/cis* relation was approximately 7/1, corresponding to the expected *trans/cis* ratio for flexible linear peptides (23). By contrast, in the scrambled sequence and the D-$Ala_{6,7}$ analog the

populations around W3-P4 and dA7-P8 *trans/cis* bond were much more similar than in the wild type peptide (1.5-2/1). A similar effect was observed in other linear peptides when a Pro residue is preceded by an aromatic amino acid (23), as is the case for the scrambled sequence. Also, in the native state of proteins there is a marked trend for an aromatic amino acid to precede a *cis* proline. In all four peptides tested, the equilibria were not significantly affected in the presence of 30% TFE.

3D structure in solution

The 3D structures of α-pheromone and its derived peptides (*trans* X-P major form) in water and TFE mixtures were calculated based on the NMR data (Fig. 6). Table 1 shows the main structural statistics of the calculations. In H_2O, α-pheromone adopted a β-turn structure comprising residues W4-R5-G6-Q7 (Fig. 6A). The turn is very well determined with a RMSD of 0.35 Å for the backbone atoms. In contrast, the N- and C-termini (W1-C2-T3 and P8-C9-W10), particularly the side-chains, were more flexible and disordered, and failed to adopt defined conformations. No side-chain interactions were found to stabilize the turn. In H_2O/TFE (Fig. 6B), the NOE data of α-pheromone are compatible with a main globular conformation. This preferred fold was a well-packed β-hairpin like structure, composed by two strands W1-C2-T3 and P8-C9-W10 linked through a β-turn formed by W4-R5-G6-Q7. The backbone and all side chains were very well determined (Table 1) and all the phi and psi angles were located within the permitted region of the Ramachandran plot. The structure is stabilized by a medium distance hydrogen bond between the backbone NH of Q7 and the O of W4. Interestingly, π-π interactions between the aromatic rings of W1 and W10 also appeared to play an important role in peptide stabilization. Regarding electrostatics, the positive R5 side chain charge (in the middle of the β-turn) was oriented towards the solvent and away from other peptide groups in water.

The scrambled peptide (*trans* W-P major form) failed to adopt a completely folded structure either in H_2O or in TFE/H_2O mixtures (Fig. 6C-D). In water, the structure was mainly random with some tendency to form a β-turn centred at C5-C6. Compared with the wild type peptide the conformational ensemble of the scrambled peptide in water was less ordered, the RMSD values were higher and the hydrophobic side chains projected towards the solvent to a higher degree. In H_2O/TFE, the central turn was stabilized and the structural convergence was slightly better. Similar to the wild type peptide, the structure of the D-$Ala_{1,2}$ analogue in H_2O, showed a turn centred at W4-Q7 and was more compact in TFE, even though it lacks the tryptophan at position W1 (Fig. 6E-F). In this case the structure was only stabilized by the hydrogen bond of the turn between the backbone atoms of W4 and Q7. By contrast, the D-$Ala_{6,7}$ analog showed a strikingly different behaviour. This sequence could not bend and behaved as a linear unfolded peptide, without any secondary structure in either solvent (Fig. 6G-H). The tendency of this analog to adopt a linear conformation is in accordance with previous studies reporting that substitution of two adjacent L-amino acids of a potentially helical peptide by the corresponding D-isomers resulted in a reduced structure and increased water accessibility and flexibility (24).

In summary, the central β-turn, although populated to varying degrees, was detected in all tested peptides except the D-$Ala_{6,7}$ analog, where the two consecutive D-Ala residues at positions 6 and 7 prevented bending. In general, all peptides were more ordered in TFE mixtures suggesting that the cosolvent stabilizes the preformed conformations. Importantly, these results indicate that *F. oxysporum* α-pheromone could adopt different structures, being more extended or flexible in the diluted conditions that favour induced fit recognition such as the extracellular environment.

Discussion

Elucidation of 3D-structures has been widely used to study structure-function relationships in small biologically active peptides (1,25,26). NMR analysis of *S. cerevisiae* α-pheromone suggested that the residues close to the N-terminus are important for receptor activation while those at the C-terminus are implicated in receptor binding, and those in the center are required for orienting the signalling and binding domains of the pheromone (1). Moreover, the central region encompassing residues K7-P8-G9-Q10 was shown to form a transient Type II

β-turn which is required for activation of Ste2 (1). These results revealed that even a relatively short peptide contains regions associated with distinct biological functions. So far, however, the lack of a high atomic resolution structure has prevented atomic modelling of the pheromone-receptor interaction.

In this work we performed structure-function analysis of the mating pheromone α from the fungal pathogen *F. oxysporum*. Such information is crucial to understand how this small peptide interacts with and activates its cognate GPCR Ste2, which was recently shown to play a key role in chemotropic growth of *F. oxysporum* towards both α-pheromone and the host plant tomato (12,27). Similar to most α-pheromones from filamentous ascomycetes (13), the *F. oxysporum* peptide is significantly shorter than its yeast counterpart. In addition, *F. oxysporum* α-pheromone contains two cysteines that could potentially be involved in inter- or intramolecular disulfide bonds, while the *S. cerevisiae* α-factor has two prolines one of which was shown to be involved in the central β-turn structure (1).

Structural characteristics of F. oxysporum α-pheromone

In spite of the difference in length, *S. cerevisiae* and *F. oxysporum* α-pheromones share a number of common features. Both are cationic peptides with a pI around 8. Both have, at the center of the ordered β-turn, a charged residue (Arg in *F. oxysporum* and Lys in *S. cerevisiae*) whose side chains point towards the solvent, suggesting that these residues may act as a molecular antenna, playing a key role in regulating potential intermolecular interactions. An interesting feature that differentiates *F. oxysporum* α-pheromone from its ortholog in *S. cerevisiae* is the presence of two cysteines, both of which were found to be reduced *in vitro*. Although it is currently unknown whether this result reflects the biological context of the pheromone-receptor interaction, the finding that the cysteines are not involved in the formation of intra- or inter-disulphide bonds together with the high reactivity and known biological functions of the thiol groups opens the intriguing hypothesis that *F. oxysporum* α-pheromone may have a previously unreported function in redox regulated processes, while *S. cerevisiae* pheromone which lacks the cysteines would not. Cysteines can easily function as nucleophiles and thus could form covalent adducts with different molecules such as lipids or ADP, a hypothesis which might be of interest for future investigations.

3D-structure of α-pheromone reveals the presence of a central β-turn essential for chemoattractant activity

The 3D-structure of *F. oxysporum* α-pheromone resembles that of the longer α-factor of *S. cerevisiae*. Both peptides contain a central β-turn with a cationic amino acid residue, Lys in *S. cerevisiae* and Arg in *F. oxysporum.* A low-resolution model for *S. cerevisiae* α-factor bound to Ste2 was previously proposed based on biochemical and biophysical data (28). The model places α-factor bent around the Pro-Gly center of the peptide, with the Lys side chain facing away from the transmembrane domains and interacting with a binding pocket formed by the extracellular loops of the receptor. A similar model could be proposed for *F. oxysporum* α-pheromone in the interaction with its cognate receptor. Although the structure of the peptide in the complex could be modified with respect to the free form (i.e. X-Pro cis/trans equilibrium) by an interacting induced fit, the presence of a preferred conformation in solution should be energetically favourable for the process.

Previous studies revealed that α-pheromone elicits a robust chemotropic response in germ tubes of *F. oxysporum*, which is dependent on the cognate GPCR Ste2 (12,29). Here we found that chemoattraction requires the G6 and Q7, but not the W1 and C2 residues of α-pheromone. This is in line with the structural role of G6 and Q7 in the maintenance of the 3D-structure, and strongly suggests that activation of Ste2-mediated chemotropic growth depends on the secondary β-turn structure of α-pheromone rather than on its amino acid composition or pI. The idea is further supported by the finding that the N-terminal W1 and C2 residues which play no substantial role in the structure of α-pheromone, are not required for chemoattraction. Indeed, alanine substitutions at the N-terminus of α-pheromone in *S. cerevisiae* and *C. albicans* led to increased pheromone activity, suggesting that this region could have an inhibitory function role in receptor-mediated signalling (1,10).

Besides chemoattraction, α-pheromone triggers a cell cycle and growth arrest in *S. cerevisiae* and *C. albicans* (30,31). Here we found that hyphae exposed to α-pheromone contained fewer cell compartments and nuclei, indicating that, similar to *S. cerevisiae* and *C. albicans* (5,32), α-pheromone inhibits cell division in *F. oxysporum*. In both *S. cerevisiae* and *C. albicans* α-pheromone inhibits cell cycle progression via Ste2-mediated activation of a dedicated signaling cascade (33-36). Unexpectedly, pheromone–mediated growth inhibition of *F. oxysporum* germ tubes does not require the cognate receptor Ste2. These results suggest the presence of additional, currently unknown α-pheromone ligands or receptors in this species, with differential roles in regulation of cell growth and chemotropism. Interestingly, the growth inhibitory activity was abolished in the D-Ala$_{1,2}$ and the scrambled analogs both of which lack a tryptophan residue at the N- or the C-terminus, respectively. Aromatic residues, particularly tryptophan, have been reported to undergo specific interactions with lipid moieties resulting in anchoring to the membrane (37). The presence of the tryptophan residues W1 and W10 at the two termini suggests that they could act as a structural clamp during a potential membrane interaction linked to the growth inhibitory activity of the α-pheromone.

In summary our results establish that *F. oxysporum* α-pheromone adopts a defined secondary structure and, despite its shorter size, contains discrete regions involved in different biological processes such as polarity reorientation and cell cycle control. We consider it likely that these findings apply to α-pheromones from other ascomycetes. The signalling functions of fungal sex pheromones might thus be more complex than previously anticipated.

Experimental Procedures

Fungal strains and culture conditions

Fusarium oxysporum f. sp. *lycopersici* strain 4287 (race 2) was used in all experiments. Generation and molecular characterization of the *F. oxysporum* FoH1-ChFP strain constitutively expressing chFP fused to histone 1 and the *ste2*Δ mutant was described previously (12,38). Fungal strains were stored as microconidial suspensions with 30% glycerol at -80°C. Strain culture and microconidia production were performed as previously described (39).

Quantification of fungal chemotropism

To measure the directed growth of *F. oxysporum* germ tubes towards gradients of synthetic peptides a chemotropic plate assay was used. Plate preparation, chemoattractant application and scoring were performed as described (12). For each concentration of test compound 5 independent batches of cells (n = 100 cells per batch) were scored. Each set of measurements was repeated in 2 independent experiments. Statistical analysis was conducted using t-test. Directed growth was quantified with an Olympus binocular microscope (Olympus Iberia, Barcelona, Spain) (200 X magnification).

For the synthesis of the scrambled peptide, 10 different scrambled α–pheromone sequences were generated using the free Scrambled software (Mimotopes, Victoria, Australia). Among these, a sequence that did not carry the conserved N-terminal Trp1-Cys2 and the central Gly6-Gln7 dipeptide residues, was selected for synthesis.

Synthetic *F. oxysporum* α–pheromone (WCTWRGQPCW), a scrambled version thereof (WRWPCCWGQT) and the di-alanine substituted analogues D-Ala$_{1,2}$ and D-Ala$_{6,7}$ were obtained from GenScript (Piscataway, NJ, USA). Lyophilized peptides were dissolved in 50% (v/v) methanol and assayed at the indicated concentrations.

Concentrations of synthetic α–pheromone and its analogs varying from 8 μM to 4 mM were chosen to cover the complete range of directional responses towards the chosen peptides. A significant chemotropic response was typically observed at a concentration of α–pheromone of 95 μM, which is higher than in some reports published in *S. cerevisiae* (40,41), albeit similar or lower to those described in *Candida* spp. to elicit pheromone response phenotypes (10,35,36,42). The discrepancy in pheromone concentration may be due to the different experimental setup of the chemotropism assays used in *Fusarium* and *Saccharomyces* (in our study pheromone gradients were established over mm rather than μm distances), differences between biological systems (multicellular versus unicellular

organism), pheromone adsorption to the agar surface, or different temperature conditions.

Quantification of germ tube length, cell compartments and nuclei

Freshly obtained microconidia of the *F. oxysporum* FoH1-ChFP strain and of the *ste2*Δ mutant were embedded in 5 ml water agarose (WA; 2%, w/v) (Pronadisa, Madrid, Spain) at a final concentration of 2.5×10^6 conidia ml^{-1} and poured into a standard Petri dish. A central scoring line was drawn on the bottom of the plate, and a parallel well was cut into the WA layer at 5 mm distance from the scoring line and filled with 40 µl of either 378 µM or 756 µM of the tested peptide. As a negative control, α–pheromone was treated with 1 mg ml^{-1} trypsin (Sigma) overnight at 37 °C and incubated for 20 min at 100 °C to remove protease activity. Plates were maintained at 28 °C in the dark for 14 hours. A 1 x 1 cm square of WA was then transferred from the plate to a microscope glass slide, and the position of the scoring line and the chemoattractant well was marked with two parallel lines on the bottom of the glass slide. To visualize septa, a 10 µl drop of 0.005% (w/v) calcofluor white (CFW) (Sigma-Aldrich, Madrid, Spain) was added on the WA, a coverslip applied on top, and samples were incubated for 5 min in the dark. Staining of nuclei in the *ste2*Δ mutant was accomplished by supplementing the CFW solution with propidium iodide (12.5 µg ml^{-1}) (Sigma-Aldrich) and RNAse A (20 µg ml^{-1}) (Sigma-Aldrich). Observation of red fluorescent nuclei and CFW-stained septa was carried out using a Zeiss Axio Imager M2 microscope (Zeiss, Barcelona, Spain) equipped with an Evolve Photometrics EM512 digital camera (Photometrics Technology, Tucson, AZ, USA). Examination using epifluorescence (1000 X magnification) was performed with UV-light 340 to 380 nm and the following filter blocks: CFW staining (G 365, FT 395, LP 420), ChFP (BP 560/40, FT 585, BP 630/75). Images were captured using the Axiovision 4.8 software (Zeiss). The length of germ tubes growing on the central scoring line was measured from photographs, using the ImageJ software (43). For each treatment a total of 50 germ tubes were measured. All experiments were performed at least four times. Statistical analysis was conducted using t-test.

Peptide oligomerization

Peptide oligomerization of *F. oxysporum* α pheromone and its analogs (75 µM) was studied in 50 mM sodium phosphate buffer (pH 7.0) in the presence and in the absence of the reducing agent dithiothreitol (DTT, 40 mM). Samples were immediately loaded, and their behaviour on a SuperPac Pep-S C2/C18 column (5 µm; 4 x 250 mm) was registered on an HPLC Beckman System Gold system. Elution was achieved with a 5 min linear gradient of 0–35% (v/v) acetonitrile gradient in 0.1% (v/v) trifluoracetic acid, followed by a second one of 35-50% in 50 min. The absorbance was monitored at 280 nm with a Beckman detector module 166. Integration of the peaks and analysis of the results were accomplished with the Beckman System Gold software (44).

Circular dichroism

Far-UV spectra were recorded on a Jasco J-715 spectropolarimeter (Easton, MD) in 0.1 cm optical path quarts cells. The results are expressed as mean residue weight ellipticities in units of degree x cm^2 x $dmol^{-1}$. The mean residue weight employed was 132.2 Da, calculated from their respective amino acid sequences. Peptides were dissolved in 50 mM sodium phosphate (with or without 30% TFE) pH 7.0, at a concentration of 80 µM. Ellipticity at 222 nm was also recorded as a function of different pH values (from 3.0 to 10.5) and salt concentrations (NaCl, $CaCl_2$ or $MgCl_2$) in the range of 0-200 mM (45).

Nuclear magnetic resonance (NMR)

NMR samples were prepared at a concentration of 0.1-0.5 mM of peptide in H_2O and H_2O/TFE (7/3 v/v) (TFE D_3 Eurisotop, France) and pH 5.0. Spectra were recorded at 5 ºC and 25 ºC on a Bruker spectrometer equipped with a cryoprobe and operating at 800 MHz for the proton.

All peptides exhibit limited solubility in H_2O and are generally more soluble in H_2O/TFE mixtures. In some cases, this fact difficulted the evaluation of weak NOE signals and the complete assignment of signals from the *cis* isomer in the equilibrium.

Phase-sensitive two-dimensional correlated spectroscopy (COSY), total correlated spectroscopy (TOCSY) and nuclear Overhauser enhancement spectroscopy (NOESY) spectra

were recorded by standard techniques using the time-proportional phase increment mode. Water signal was suppressed by either presaturation or by using a 3–9–19 pulse sequence. TOCSY spectra were obtained by using a DIPSI2 pulse sequence with a 60 ms mixing time and with a z filter spin-lock sequence. The NOESY mixing time was 150 ms. ^{1}H-^{13}C heteronuclear single quantum coherence (HSQC) spectra were recorded at ^{13}C natural abundance. Data were processed with the standard TOPSPIN program (Bruker Biospin, Karlsruhe, Germany). The 2D data matrices were multiplied by a square-sine-bell window function with the corresponding shift optimised for every spectrum and zero-filled to 2×1 K complex matrices prior to Fourier transformation. Baseline correction was applied in both dimensions. The ^{13}C δ-values were indirectly referenced by using the IUPAC-IUB recommended ^{1}H/^{13}C chemical shift ratio (46).

Assignments of the ^{1}H spectra in both solvents were obtained following the sequential assignment protocols (47) with the help of the SPARKY software (48). The ^{13}C resonances were identified on the basis of the correlations between the protons and the bound carbon atoms present in the ^{1}H-^{13}C-HSQC spectra.

Structure calculations of the major *trans* X-P bond conformers were performed with CYANA 2.1 program (49). NOE integrated cross-peaks were translated into distance restraints, and the Φ and Ψ dihedral angle restraints were obtained using TALOS + webserver (50). Typically 200 structures were calculated using a standard protocol. The lists of distance constraints were checked with the corresponding NOESY spectra, ambiguous constraints were relaxed or removed in order to generate a final list used as input for a standard simulated annealing CYANA 2.1 calculation. The 20 conformers with the lowest target function values were selected. The structural ensembles were visualized and examined using MOLMOL (51) and PyMOL (52).

Acknowledgements: The authors acknowledge financial support by the Spanish Ministerio de Economía y Competitividad (MINECO) through projects CTQ2014-52633-P, BFU2012-32404 and BIO2013-47870-R. S.V. is supported by Marie Curie ITN FUNGIBRAIN (FP7-PEOPLE-ITN-607963) from the European Commission. A.P.-H. is recipient of a predoctoral fellowship 579971 from CONACYT.

Conflict of interest: The authors declare that they have no conflicts of interest with the contents of this article.

Author contributions: SV designed, performed and analyzed the experiments in Figures 1-4 and wrote the paper. APH and SS performed and analyzed the NMR experiments and structure calculations in Figures 5-6. AMP designed, performed and analyzed the experiments in Figures 4 and wrote the paper. ADP coordinated the study and wrote the paper. DT conceived and coordinated the study and wrote the paper. MB conceived and coordinated the study and wrote the paper. All authors analyzed the results and approved the final version of the manuscript.

References

1. Naider, F., and Becker, J. M. (2004) The alpha-factor mating pheromone of Saccharomyces cerevisiae: a model for studying the interaction of peptide hormones and G protein-coupled receptors. *Peptides* **25**, 1441-1463
2. Jones, S. K., Jr., and Bennett, R. J. (2011) Fungal mating pheromones: choreographing the dating game. *Fungal Genet Biol* **48**, 668-676
3. Arkowitz, R. A. (2009) Chemical gradients and chemotropism in yeast. *Cold Spring Harb Perspect Biol* **1**, a001958
4. Segall, J. E. (1993) Polarization of yeast cells in spatial gradients of alpha mating factor. *Proc Natl Acad Sci U S A* **90**, 8332-8336
5. Bucking-Throm, E., Duntze, W., Hartwell, L. H., and Manney, T. R. (1973) Reversible arrest of haploid yeast cells in the initiation of DNA synthesis by a diffusible sex factor. *Exp Cell Res* **76**, 99-110
6. Kurjan, J., and Herskowitz, I. (1982) Structure of a yeast pheromone gene (MF alpha): a putative alpha-factor precursor contains four tandem copies of mature alpha-factor. *Cell* **30**, 933-943
7. Venkatachalam, C. M. (1968) Stereochemical criteria for polypeptides and proteins. V. Conformation of a system of three linked peptide units. *Biopolymers* **6**, 1425-1436
8. Chou, P. Y., and Fasman, G. D. (1979) Prediction of beta-turns. *Biophys J* **26**, 367-383
9. Shenbagamurthi, P., Kundu, B., Raths, S., Becker, J. M., and Naider, F. (1985) Biological activity and conformational isomerism in position 9 analogues of the des-1-tryptophan,3-beta-cyclohexylalanine-alpha-factor from Saccharomyces cerevisiae. *Biochemistry* **24**, 7070-7076
10. Alby, K., and Bennett, R. J. (2011) Interspecies pheromone signaling promotes biofilm formation and same-sex mating in Candida albicans. *Proc Natl Acad Sci U S A* **108**, 2510-2515
11. Pöggeler, S. (2011) 5 Function and Evolution of Pheromones and Pheromone Receptors in Filamentous Ascomycetes. in *Evolution of Fungi and Fungal-Like Organisms* (Pöggeler, S., and Wöstemeyer, J. eds.), Springer Berlin Heidelberg, Berlin, Heidelberg. pp 73-96
12. Turra, D., El Ghalid, M., Rossi, F., and Di Pietro, A. (2015) Fungal pathogen uses sex pheromone receptor for chemotropic sensing of host plant signals. *Nature* **527**, 521-524
13. Martin, S. H., Wingfield, B. D., Wingfield, M. J., and Steenkamp, E. T. (2011) Causes and consequences of variability in peptide mating pheromones of ascomycete fungi. *Mol Biol Evol* **28**, 1987-2003
14. Dean, R., Van Kan, J. A., Pretorius, Z. A., Hammond-Kosack, K. E., Di Pietro, A., Spanu, P. D., Rudd, J. J., Dickman, M., Kahmann, R., Ellis, J., and Foster, G. D. (2012) The Top 10 fungal pathogens in molecular plant pathology. *Molecular plant pathology* **13**, 414-430
15. Roccatano, D., Colombo, G., Fioroni, M., and Mark, A. E. (2002) Mechanism by which 2,2,2-trifluoroethanol/water mixtures stabilize secondary-structure formation in peptides: a molecular dynamics study. *Proceedings of the National Academy of Sciences of the United States of America* **99**, 12179-12184
16. Jimenez, M. A., Bruix, M., Gonzalez, C., Blanco, F. J., Nieto, J. L., Herranz, J., and Rico, M. (1993) CD and 1H-NMR studies on the conformational properties of peptide fragments from the C-terminal domain of thermolysin. *European journal of biochemistry / FEBS* **211**, 569-581
17. Buck, M. (1998) Trifluoroethanol and colleagues: cosolvents come of age. Recent studies with peptides and proteins. *Quarterly reviews of biophysics* **31**, 297-355
18. Wade, D., Boman, A., Wahlin, B., Drain, C. M., Andreu, D., Boman, H. G., and Merrifield, R. B. (1990) All-D amino acid-containing channel-forming antibiotic peptides. *Proceedings of the National Academy of Sciences of the United States of America* **87**, 4761-4765

19. Wishart, D. S., and Sykes, B. D. (1994) The 13C chemical-shift index: a simple method for the identification of protein secondary structure using 13C chemical-shift data. *Journal of biomolecular NMR* **4**, 171-180
20. Perkins, S. J., and Wuthrich, K. (1979) Ring current effects in the conformation dependent NMR chemical shifts of aliphatic protons in the basic pancreatic trypsin inhibitor. *Biochimica et biophysica acta* **576**, 409-423
21. Wishart, D. S., Bigam, C. G., Holm, A., Hodges, R. S., and Sykes, B. D. (1995) (1)H, (13)C and (15)N random coil NMR chemical shifts of the common amino acids. I. Investigations of nearest-neighbor effects. *Journal of biomolecular NMR* **5**, 332
22. Schubert, M., Labudde, D., Oschkinat, H., and Schmieder, P. (2002) A software tool for the prediction of Xaa-Pro peptide bond conformations in proteins based on 13C chemical shift statistics. *Journal of biomolecular NMR* **24**, 149-154
23. Grathwohl, C., and Wuthrich, K. (1976) Nmr studies of the molecular conformations in the linear oligopeptides H-(L-Ala)n-L-Pro-OH. *Biopolymers* **15**, 2043-2057
24. Rothemund, S., Beyermann, M., Krause, E., Krause, G., Bienert, M., Hodges, R. S., Sykes, B. D., and Sonnichsen, F. D. (1995) Structure effects of double D-amino acid replacements: a nuclear magnetic resonance and circular dichroism study using amphipathic model helices. *Biochemistry* **34**, 12954-12962
25. Grieco, P., Luca, V., Auriemma, L., Carotenuto, A., Saviello, M. R., Campiglia, P., Barra, D., Novellino, E., and Mangoni, M. L. (2011) Alanine scanning analysis and structure-function relationships of the frog-skin antimicrobial peptide temporin-1Ta. *J Pept Sci* **17**, 358-365
26. Cunningham, B. C., and Wells, J. A. (1989) High-resolution epitope mapping of hGH-receptor interactions by alanine-scanning mutagenesis. *Science* **244**, 1081-1085
27. Turra, D., and Di Pietro, A. (2015) Chemotropic sensing in fungus-plant interactions. *Curr Opin Plant Biol* **26**, 135-140
28. Lee, B. K., Khare, S., Naider, F., and Becker, J. M. (2001) Identification of residues of the Saccharomyces cerevisiae G protein-coupled receptor contributing to alpha-factor pheromone binding. *J Biol Chem* **276**, 37950-37961
29. Turra, D., Nordzieke, D., Vitale, S., El Ghalid, M., and Di Pietro, A. (2016) Hyphal chemotropism in fungal pathogenicity. *Semin Cell Dev Biol* **57**, 69-75
30. Manney, T. R. (1983) Expression of the BAR1 gene in Saccharomyces cerevisiae: induction by the alpha mating pheromone of an activity associated with a secreted protein. *J Bacteriol* **155**, 291-301
31. Panwar, S. L., Legrand, M., Dignard, D., Whiteway, M., and Magee, P. T. (2003) MFalpha1, the gene encoding the alpha mating pheromone of Candida albicans. *Eukaryotic cell* **2**, 1350-1360
32. Jones, S. K., Jr., Clarke, S. C., Craik, C. S., and Bennett, R. J. (2015) Evolutionary Selection on Barrier Activity: Bar1 Is an Aspartyl Protease with Novel Substrate Specificity. *MBio* **6**, e01604-01615
33. Reneke, J. E., Blumer, K. J., Courchesne, W. E., and Thorner, J. (1988) The carboxy-terminal segment of the yeast alpha-factor receptor is a regulatory domain. *Cell* **55**, 221-234
34. Elion, E. A., Satterberg, B., and Kranz, J. E. (1993) FUS3 phosphorylates multiple components of the mating signal transduction cascade: evidence for STE12 and FAR1. *Molecular biology of the cell* **4**, 495-510
35. Schaefer, D., Cote, P., Whiteway, M., and Bennett, R. J. (2007) Barrier activity in Candida albicans mediates pheromone degradation and promotes mating. *Eukaryotic cell* **6**, 907-918
36. Lin, C. H., Choi, A., and Bennett, R. J. (2011) Defining pheromone-receptor signaling in Candida albicans and related asexual Candida species. *Molecular biology of the cell* **22**, 4918-4930

37. de Jesus, A. J., and Allen, T. W. (2013) The role of tryptophan side chains in membrane protein anchoring and hydrophobic mismatch. *Biochimica et biophysica acta* **1828**, 864-876
38. Ruiz-Roldan, M. C., Kohli, M., Roncero, M. I., Philippsen, P., Di Pietro, A., and Espeso, E. A. (2010) Nuclear dynamics during germination, conidiation, and hyphal fusion of Fusarium oxysporum. *Eukaryotic cell* **9**, 1216-1224
39. Di Pietro, A., Garcia-MacEira, F. I., Meglecz, E., and Roncero, M. I. (2001) A MAP kinase of the vascular wilt fungus Fusarium oxysporum is essential for root penetration and pathogenesis. *Mol Microbiol* **39**, 1140-1152
40. Paliwal, S., Iglesias, P. A., Campbell, K., Hilioti, Z., Groisman, A., and Levchenko, A. (2007) MAPK-mediated bimodal gene expression and adaptive gradient sensing in yeast. *Nature* **446**, 46-51
41. Gelin-Licht, R., Paliwal, S., Conlon, P., Levchenko, A., and Gerst, J. E. (2012) Scp160-dependent mRNA trafficking mediates pheromone gradient sensing and chemotropism in yeast. *Cell reports* **1**, 483-494
42. Dignard, D., and Whiteway, M. (2006) SST2, a regulator of G-protein signaling for the Candida albicans mating response pathway. *Eukaryotic cell* **5**, 192-202
43. Schneider, C. A., Rasband, W. S., and Eliceiri, K. W. (2012) NIH Image to ImageJ: 25 years of image analysis. *Nat Methods* **9**, 671-675
44. Wirth, J., Martinez del Pozo, A., Mancheno, J. M., Martinez-Ruiz, A., Lacadena, J., Onaderra, M., and Gavilanes, J. G. (1997) Sequence determination and molecular characterization of gigantin, a cytotoxic protein produced by the mould Aspergillus giganteus IFO 5818. *Archives of biochemistry and biophysics* **343**, 188-193
45. de Antonio, C., Martinez del Pozo, A., Mancheno, J. M., Onaderra, M., Lacadena, J., Martinez-Ruiz, A., Perez-Canadillas, J. M., Bruix, M., and Gavilanes, J. G. (2000) Assignment of the contribution of the tryptophan residues to the spectroscopic and functional properties of the ribotoxin alpha-sarcin. *Proteins* **41**, 350-361
46. Markley, J. L., Bax, A., Arata, Y., Hilbers, C. W., Kaptein, R., Sykes, B. D., Wright, P. E., and Wuthrich, K. (1998) Recommendations for the presentation of NMR structures of proteins and nucleic acids--IUPAC-IUBMB-IUPAB Inter-Union Task Group on the standardization of data bases of protein and nucleic acid structures determined by NMR spectroscopy. *European journal of biochemistry / FEBS* **256**, 1-15
47. Wüthrich, K. (1986) NMR of proteins and nucleic acids. *Wiley-Interscience, John Wiley & Sons*
48. Goddard, T. D., and Kneller, D. G. (2005) Sparky 3, University of California, San Francisco.
49. Guntert, P. (2004) Automated NMR structure calculation with CYANA. *Methods in molecular biology* **278**, 353-378
50. Shen, Y., Delaglio, F., Cornilescu, G., and Bax, A. (2009) TALOS+: a hybrid method for predicting protein backbone torsion angles from NMR chemical shifts. *Journal of biomolecular NMR* **44**, 213-223
51. Koradi, R., Billeter, M., and Wüthrich, K. (1996) MOLMOL: a program for display and analysis of macromolecular structures. *J Mol Graph* **14**, 51-55, 29-32
52. Schrödinger, L. (2010) The PyMOL Molecular Graphics System, Version 1.3r1.

TABLE 1. Main structural statistical parameters for the ensemble of the 20 lowest target function conformers calculated for α-pheromone, a randomly scrambled version, and the D-Ala$_{6,7}$ and D-Ala$_{1,2}$ analogs, in H_2O and 30/70 % v/v TFE/H_2O.

	Water				Water/TFE			
Pheromone	α pheromone	scrambled	D-Ala$_{1,2}$	D-Ala$_{6,7}$	α pheromone	scrambled	D-Ala$_{1,2}$	D-Ala$_{6,7}$
Upper limit distance restraints (from NOEs)	57	59	88	73	109	78	125	99
φ/ψ Dihedral angle constrains (from chemical shifts)	4	2	14	11	11	4	9	15
Averaged CYANA target function value	0.01± 0.001	0.01 ± 0.001	0.02± 0.001	0.11 ± 0.01	0.02 ± 0.004	0.11 ± 0.01	0.28 ± 0.001	0.08 ± 0.003
Averaged maximum violation per structure								
Distance (Å)	0.003	0.001	0.001	0 .001	0.002	0.001	0.001	0.009
Dihedral angle (º)	0.01	0.0	0.40	1.28	0.16	0.0	1.52	0.54
Pairwise RMSD (Å)								
Backbone atoms	1.65 ± 0.59	2.85 ± 0.96	0.66 ± 0.25	2.0 ± 0.75	0.24 ± 0.10	2.19 ± 0.85	0.96 ± 0.37	0.82 ± 0.33
All heavy atoms	3.44 ± 0.85	4.37 ± 0.98	1.61 ± 0.47	3.23 ± 0.68	0.58 ± 0.18	4.15 ± 1.15	1.93 ± 0.54	2.16 ± 0.51
Ramachandran plot (%)								
Favorable	62.5	92.5	66.2	83.8	77.5	90.8	76.2	75
Additional	37.5	7.5	33.8	16.2	22.5	9.2	23.8	25
Generous	0	0	0	0	0	0	0	0
Disallowed	0	0	0	0	0	0	0	0

Figure Legends

Figure 1. The central Gly_6 and Gln_7 residues of α-pheromone are essential for chemoattractant activity. *A-B.* Dose-response curves for directed growth of *Fusarium oxysporum* germ tubes towards synthetic *F. oxysporum* α-pheromone (α–pher) (WCTWRGQPCW), its analogs (D-$Ala_{1,2}$) and (D-$Ala_{6,7}$) (*A*); or a randomly scrambled version (WRWPCCWGQT) (*B*). *C.* Directed growth of *F. oxysporum* wt and *ste2*Δ germ tubes after 13 h exposure to a gradient of the indicated componds (versus wt, * $P < 0.0001$). For each measurement, 5 independent batches of cells (n = 100 cells per batch) were scored. Each bar represents the mean of 2 independent sets of measurements. Error bars show s.d.

Figure 2. ***F. oxysporum* α-pheromone inhibits cell division and hyphal growth in a Ste2-independent manner.** *A-D.* Number of cellular compartments and nuclei (*A-B*), or length (*C-D*) of wt (*A, C*) and *ste2*Δ (*B, D*) germ tubes was determined after 14 h exposure to a gradient of the indicated concentrations of untreated (Trp-) or trypsin-treated (Trp+) α-pheromone (α–pher) (* $P < 0.0001$). Length of germ tubes was measured using the ImageJ software and expressed as percentage relative to hyphae exposed to 378 μM Trp+ α-pher. Mean values were calculated from 4 independent experiments, each with 50 germ tubes. Error bars show s.d. *E.* Representative micrographs of *F. oxysporum* germlings whose nuclei are labelled with H1-ChFP, exposed to a gradient of untreated or Trp+ α-pher and stained with Calcofluor white (CFW). Scale bar, 10 μm.

Figure 3. **The N-terminal Trp_1 and Cys_2 residues of α-pheromone are essential for growth inhibitory activity.** *A-B.* Number of cellular compartments and nuclei (*A*), or length (*B*) of germ tubes was determined after 14 h exposure to a gradient of 378 μM α-pheromone (α–pher), its analogs (D-$Ala_{1,2}$) and (D-$Ala_{6,7}$) (*A*); or a randomly scrambled version (* $P < 0.0001$ versus the same concentration of α–pher). Length of germ tubes was measured using the ImageJ software. Mean values were calculated from 4 independent experiments, each with 50 germ tubes. Error bars show s.d. *C.* Representative micrographs of *F. oxysporum* germlings whose nuclei are labelled with H1-ChFP, exposed to a gradient of the indicated peptides and stained with Calcofluor white (CFW). Scale bar, 10 μm.

Figure 4. Structural and biophysical characterization of α-pheromone and related peptides. *A.* HPLC fractionation of *F. oxysporum* α-pheromone (left panel) or the scrambled peptide (right panel) incubated in the absence (blue line) or presence of DTT (red line). The position of the peptides and the excess of DTT are indicated with arrows. The gradient is shown as a gray thin line. *B.* Far-UV circular dichroism spectra in the absence (solid lines) or presence of 30% (v/v) TFE (dashed lines). The spectra correspond to *F. oxysporum* α-pheromone (black), the randomly scrambled peptide (red), the D-$Ala_{1,2}$ (blue) or the D-$Ala_{6,7}$ analog (green). Results are shown as mean residue weight ellipticity (θ_{MRW}) values and expressed in units of degree x cm^2 x $dmol^{-1}$.

Figure 5. Experimental ^1H and ^{13}C NMR data of *F. oxysporum* α-pheromone. *A.* Region of the ^1H-^{13}C HSQC natural abundance spectra in H_2O, showing signals corresponding to Cβ of cysteine residues (boxed) indicative of their reduced state. Other signals are also labelled. * Correspond to an impurity. *B-C.* Regions of the NOESY spectra in H_2O (*B*) and in H_2O/TFE mixture (*C*). Non sequential NOEs are labelled in black and signals belonging to Q-P *cis* conformation are in *italic*.

Figure 6. The central G_6 and Q_7 residues are crucial for defined β-turn structure in solution. Solution structure of the preferred conformation of α-pheromone and related peptides in H_2O (*A, C, E, G*) and H_2O/TFE mixture (*B, D, F, H*) calculated by NMR. The superposition of the backbone of the best 20 structures in each family is represented in grey. Side chains of the energetically best structure in solution are in different colours depending of the sequence position, 1: blue; 2: red; 3: yellow; 4:

cyan; 5: magenta; 6: grey; 7: violet; 8: orange; 9: green and 10: brown. Peptide termini are indicated by “N” and “C". Residues are labelled with the one letter code and sequence number.

Figure 1.

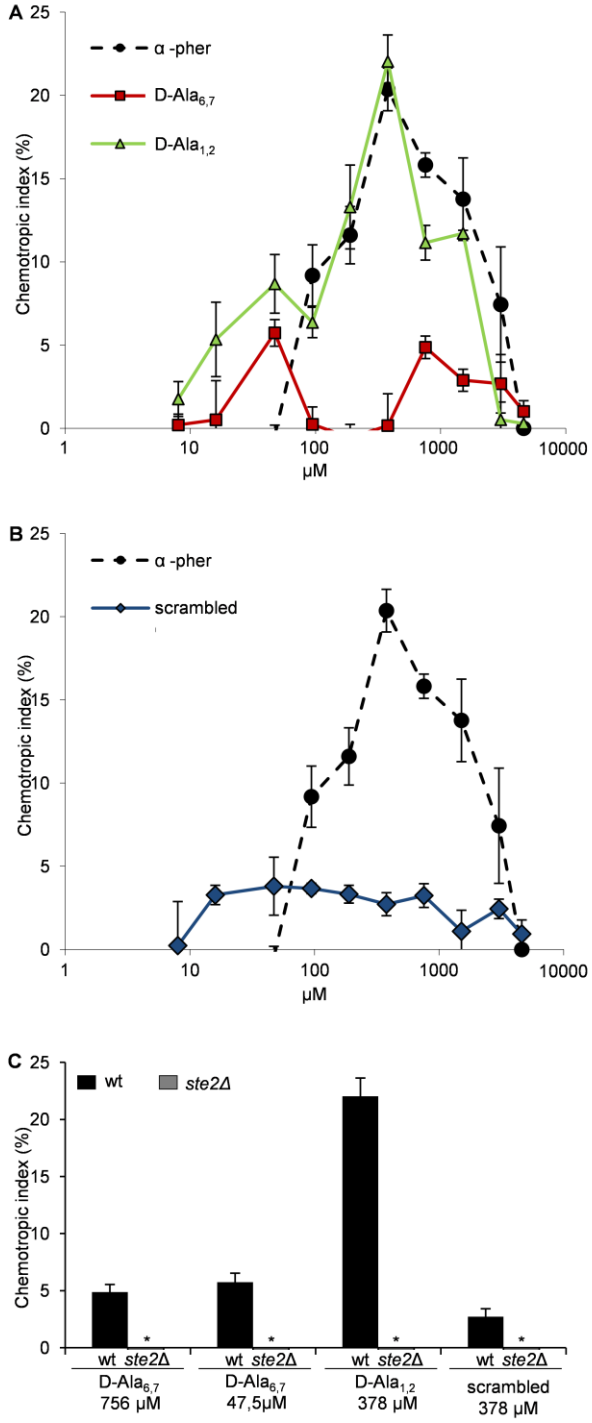

Figure 2.

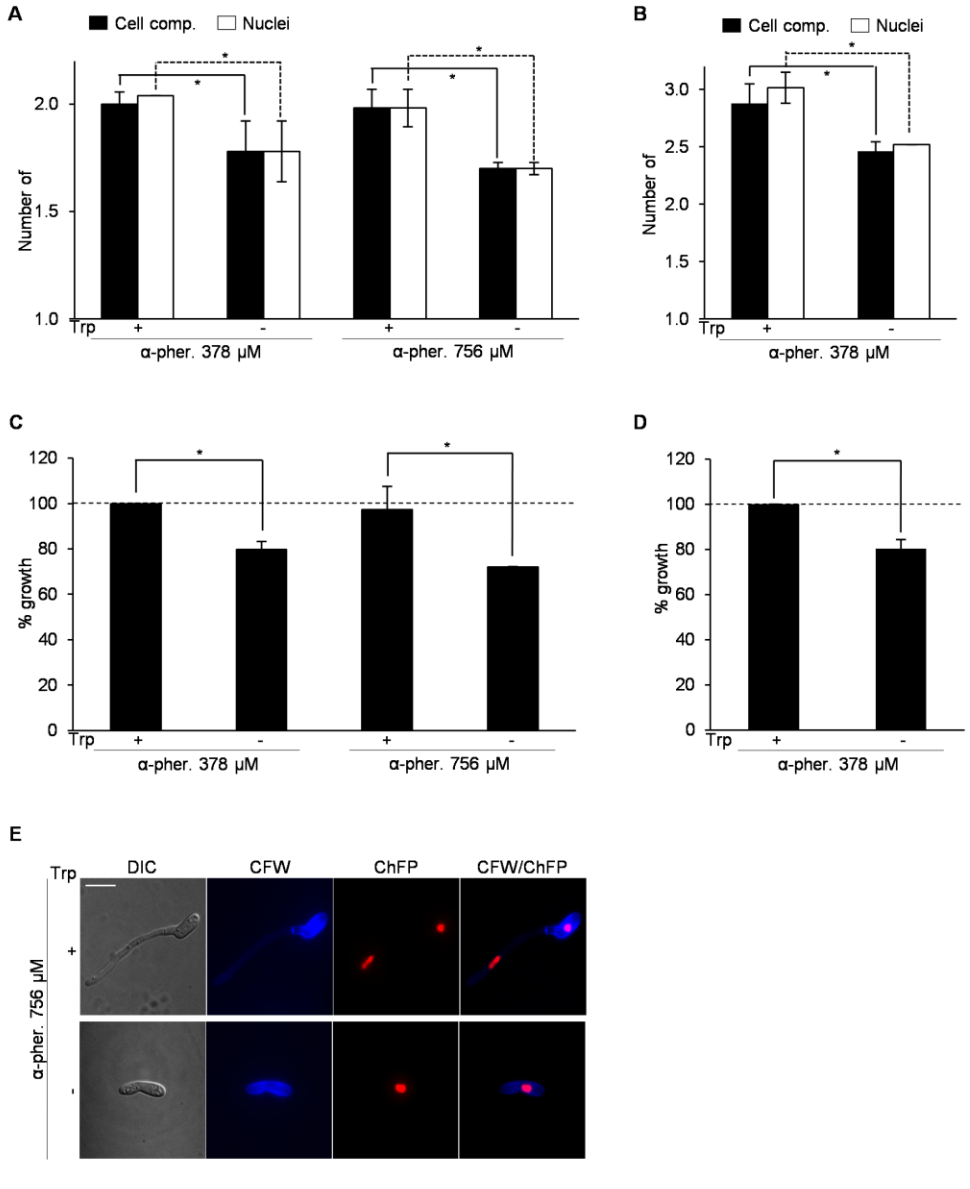

Figure 3.

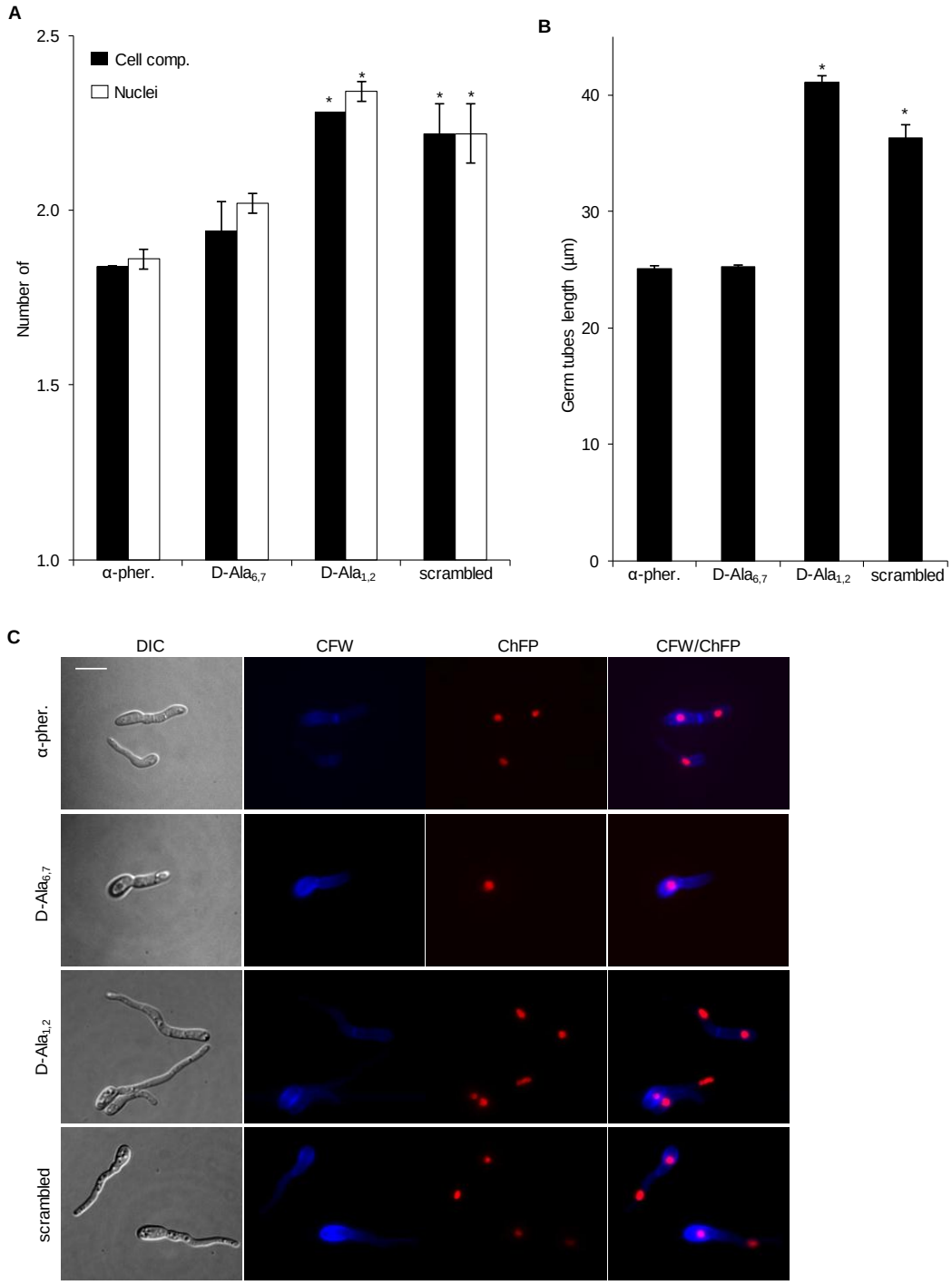

Figure 4.

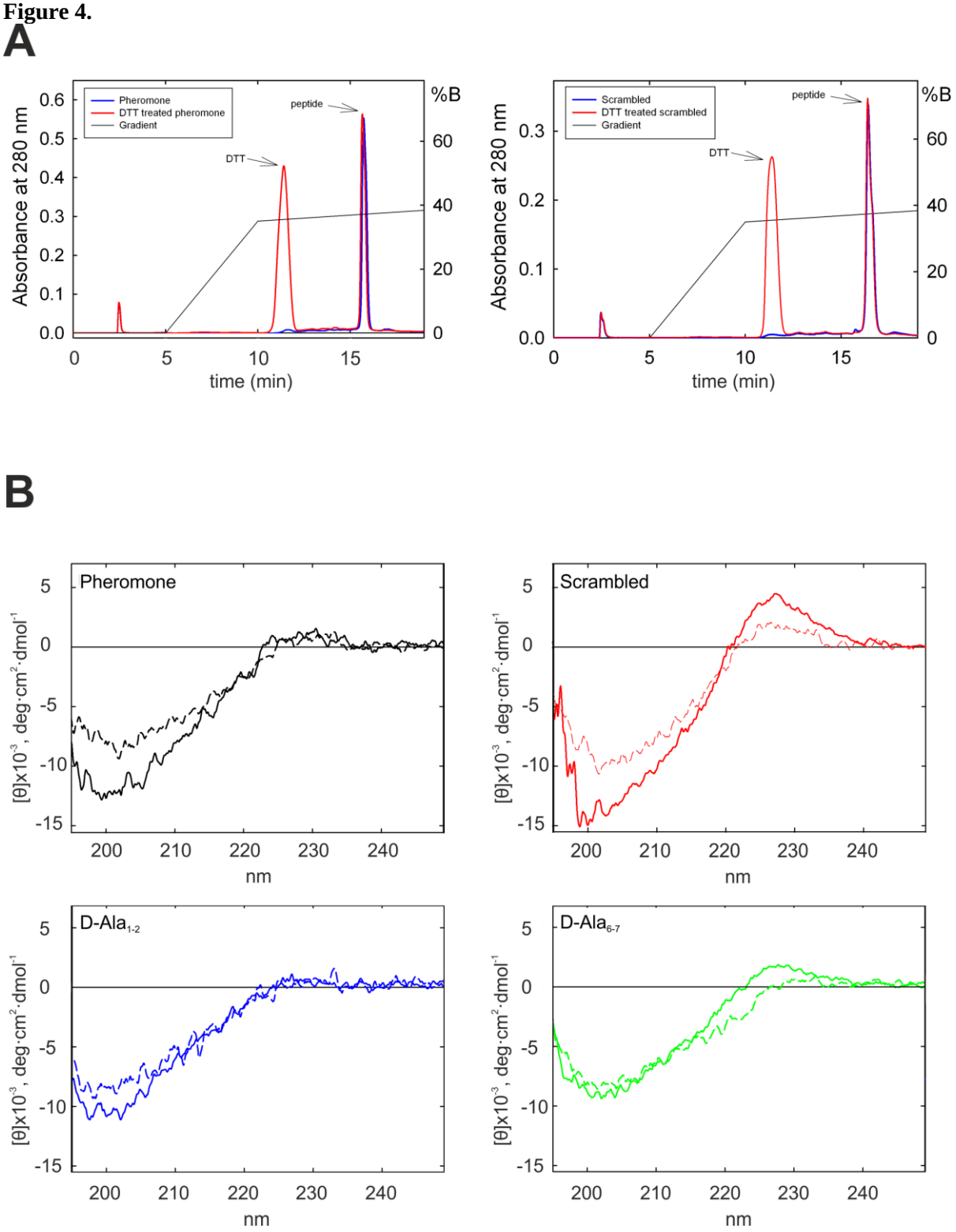

Figure 5.

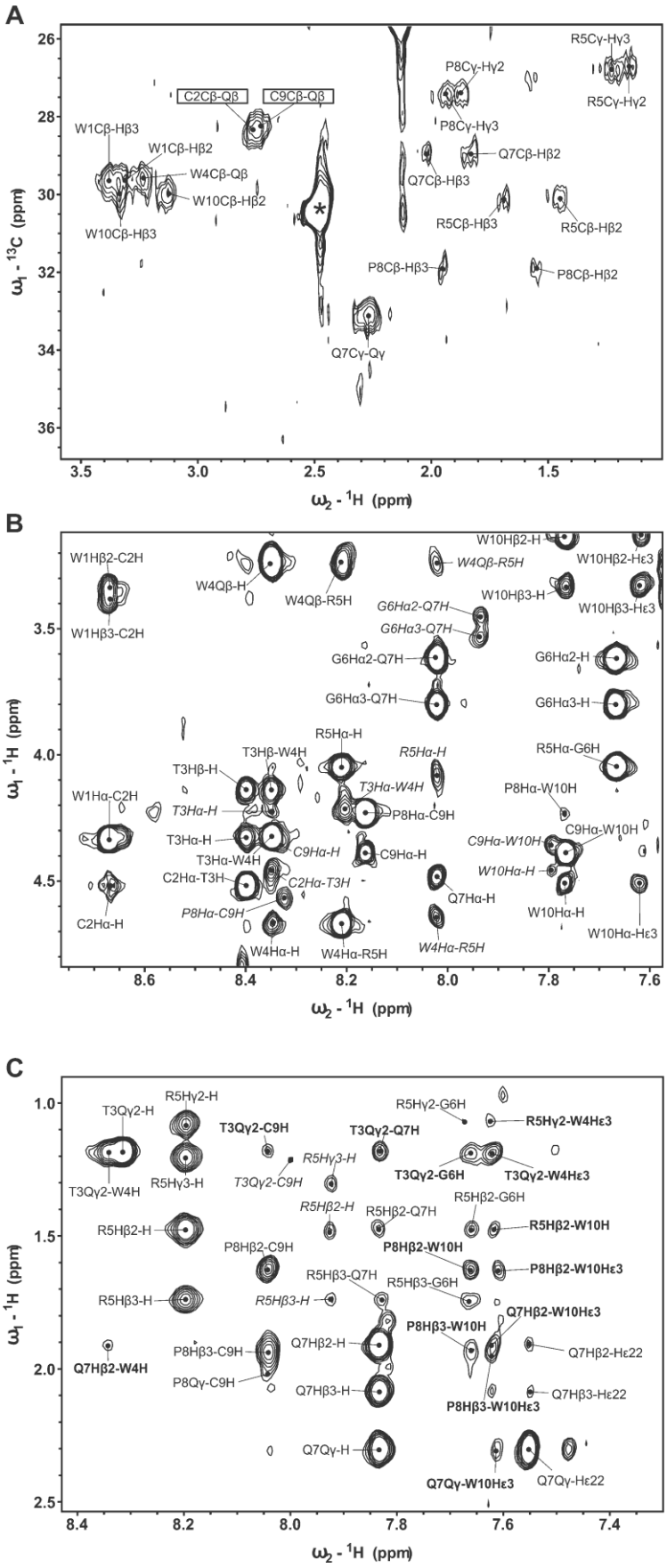

Figure 6.

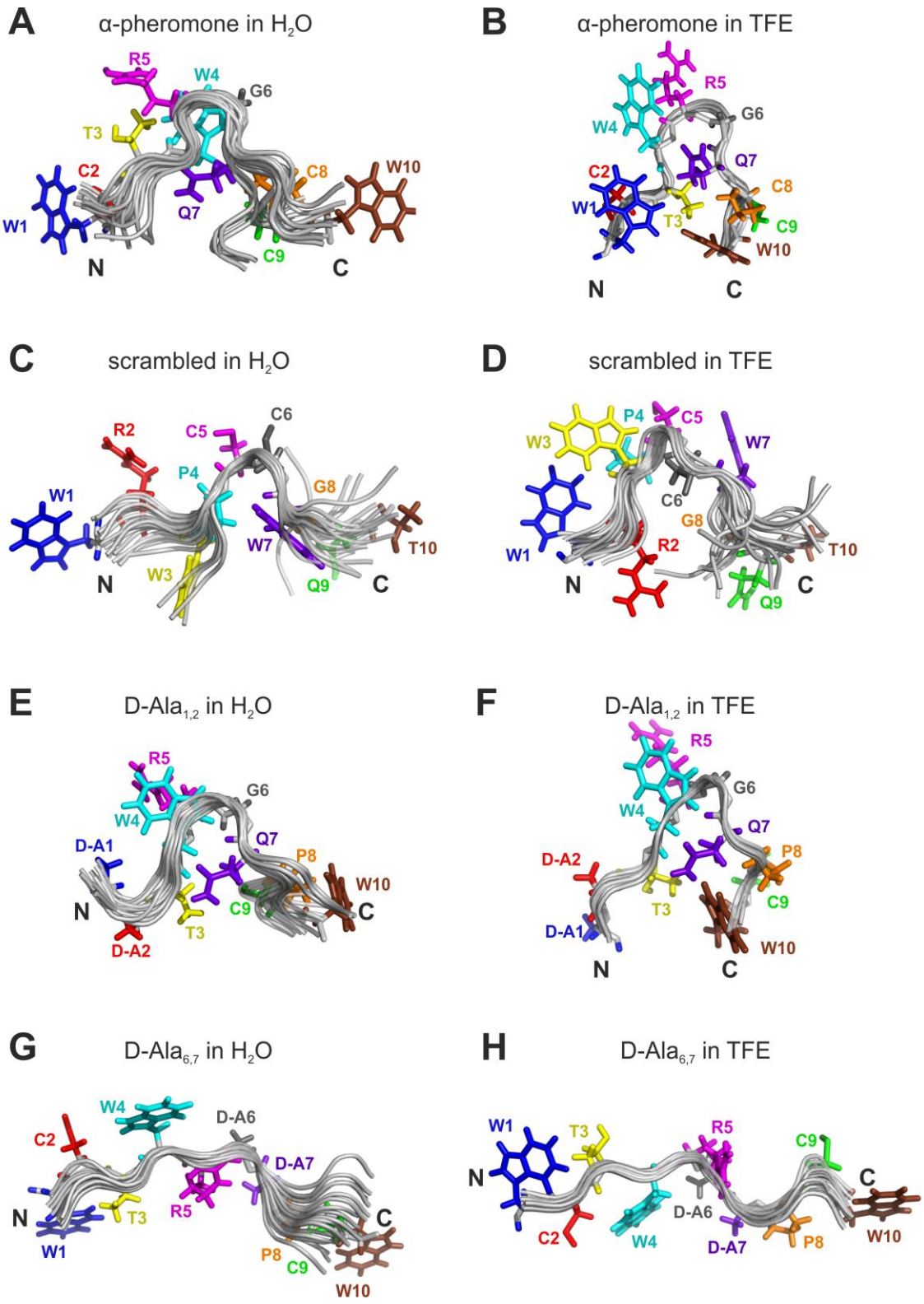

Structure-activity relationship of α mating pheromone from the fungal pathogen *Fusarium oxysporum*

Stefania Vitale, Angélica Partida-Hanon, Soraya Serrano, Álvaro Martínez-del-Pozo, Antonio Di Pietro, David Turrà and Marta Bruix

J. Biol. Chem. published online January 18, 2017

Access the most updated version of this article at doi: 10.1074/jbc.M116.766311